Electronic Supplementary Material (ESI) for Nanoscale.
This journal is © The Royal Society of Chemistry 2017

Supporting Information

One-pot Synthesis of Ni Nanoparticles/Ordered Mesoporous Carbon Composite Electrode Materials for Electrocatalytic Reduction of Aromatic Ketones

Zhi-Xia Zhang,[a] Yupu Liu,[b] Wang-Jun Meng,[a] Jinxiu Wang,[b] Wei Li,*[b] Huan Wang,*[a] Dongyuan Zhao[b] and Jia-Xing Lu*[a]

[a] Shanghai Key Laboratory of Green Chemistry and Chemical Processes, School of Chemistry and Molecular Engineering, East China Normal University, Shanghai 200062, P. R. China

[b] Department of Chemistry, Shanghai Key Laboratory of Molecular Catalysis and Innovative Materials, Laboratory of Advanced Materials, iChEM (Collaborative Innovation Center of Chemistry for Energy Materials), Fudan University, Shanghai 200433, P. R. China

1 Chemicals and instruments

All reagents were commercially available (Aldrich) and were directly used without further purification.

Activated carbon (AC) was purchased from Sinopharm Chemical Reagent Co. Ltd (Shanghai, China).

Carbon Nanotube (CNT) Multi-walled below 10 nm (diam.), 5-15 μm (length) was purchased from Tokyo Chemical Industry Co. Ltd (Shanghai, China).

The X-ray diffraction (XRD) patterns were collected on a Bruker D8 ADVANCE instrument using Cu-Kα radiation ($\lambda = 1.5418$ Å) at 35 kV and 25 mA.

Thermogravimetric analysis (TGA) was carried out using a Metzsch TGA-STA449F3 analyzer from 25 to 800°C in an air flow of 80 mL min^{-1} at a heating rate of 10°C·min^{-1}.

Nitrogen adsorption–desorption isotherms were measured on a Quancachrome Autosorb-3B instrument after evacuating the samples at 573 K for 6 h. The specific surface areas were evaluated using the Brunauer-Emmett-Teller (BET) method and the pore distribution was calculated by the BJH method from adsorption branches of isotherms.

The TEM images were recorded using a JEOL-JEM-2010 microscope after the specimens were dispersed in ethanol and placed on holey copper grids.

EDX-MAPPING were obtained on a Hitachi S-4800 field-emission scanning microscope.

The galvanostatic electrolysis was done with a dc regulated power supply HY 3001E (Hangzhou Huayi Electronics Industry Co., Ltd.).

^1H spectra were acquired on a Bruker DRX500 spectrometer at 400 MHz in $CDCl_3$ with TMS as an internal standard.

The resulting reaction mixture was analyzed by gas chromatography-mass spectrometry (GC-MS) for product identification, which was performed on an Agilent 6890 instrument equipped with an Agilent 5973 mass selective detector.

The conversion and selectivity of products were quantified on an Shimadzu GC-2014 GC equipped with a flame ionization detector and a Rtx®-5 column (30 m × 0.25 mm × 0.25 μm) using biphenyl as an internal standard.

2 Electrocatalytic Reduction of Aromatic Ketones (typical procedure)

The galvanostatic electrolysis was carried out in a mixture of substrate aromatic ketone **1** (0.025 M) and TEABr (0.1 M) in 20 mL co-solvent (DMF/EtOH = 9/1) under a slow stream of N_2 in an undivided glass cell equipped with a magnesium rod sacrificial anode and a Ni/OMC cathode until 2-4 F of charge was passed. The reaction mixture was hydrolyzed and extracted with Et_2O, and the organic layers was washed with H_2O, dried over $MgSO_4$, and filtered. The products were analyzed by gas chromatography to obtain the yields based on the starting materials.

1-(4-Methylphenyl)-1-propanol (2a) MS (EI): m/z (%) = 150 [M^+] (12), 132 (3), 122 (9), 121 (100) 119 (7), 117 (4), 115 (3), 105 (3), 94 (3), 93 (36), 92 (3), 91 (31), 78 (3), 77 (18), 65 (6), 63 (2), 57 (2), 51 (3).

3,4-Bis(4-methylphenyl)- 3,4-hexanediol (3a) MS (EI): m/z (%) = 150 (31), 149 [M/2$^+$] (100), 148 (6), 135 (10), 133 (2), 131 (4), 121 (3), 120 (4), 119 (35), 117 (3), 115 (2), 105 (4), 92 (2), 91 (20), 77 (2), 65 (5), 57 (35).

1-Phenyl-1-propanol (2b) MS (EI): m/z (%) = 136 [M$^+$] (16), 108 (8), 107 (100), 105 (8), 91 (5), 79 (54), 78 (6), 77 (29), 51 (8).

3,4-Diphenyl-3,4-hexanediol (3b) MS (EI): m/z (%)=136 (47), 135 [M/2$^+$] (100), 134 (9), 133 (14), 117 (11), 115 (8), 105 (45), 91 (14), 77 (30), 57 (38), 44 (25), 40 (12).

1-Phenylethanol (2c) MS (EI): m/z (%) = 122 [M$^+$] (38), 121 (6), 120 (6), 108 (8), 107 (100), 105 (26), 104 (9), 103 (7), 91 (6), 80 (6), 79 (88), 78 (23), 77 (65), 74 (5), 53 (7), 52 (7), 51 (21), 50 (9), 45 (5), 44 (18), 43 (22), 40 (6), 39 (7).

2,3-Diphenyl-2,3-butanediol (3c) MS (EI): m/z (%) = 122 (51), 121 [M/2$^+$] (100), 120 (9), 107 (11), 106 (6), 105 (30), 103 (8), 91 (6), 78 (12), 77 (34), 51 (12), 44 (30), 43 (80), 40 (8).

1-Methyl-3-phenyl-1-propanol (2d) MS (EI): m/z (%) = 150 [M$^+$] (8), 148 (35), 133 (11), 132 (34), 131 (7), 118 (9), 117 (75), 115 (8), 105 (48), 104 (11), 103 (14), 92 (32), 91 (100), 79 (12), 78 (30), 77 (22), 65 (15), 51 (13).

1-(4-Methylphenyl)-1-ethanol (2e) MS (EI): m/z (%) = 136 [M$^+$] (39), 121 (100), 117 (21), 93 (62), 92 (23), 91 (84), 77 (33), 65 (23), 51 (18).

2,3-Bis(4-methylphenyl)-2,3-butanediol (3e) MS (EI): m/z (%) = 136 (35), 135 [M/2$^+$] (100), 134 (7), 121 (15), 119 (19), 117 (4), 115 (4), 105 (3), 92 (3), 91 (23), 77 (4), 65 (6.).

3 Small-angle XRD pattern of FDU-16

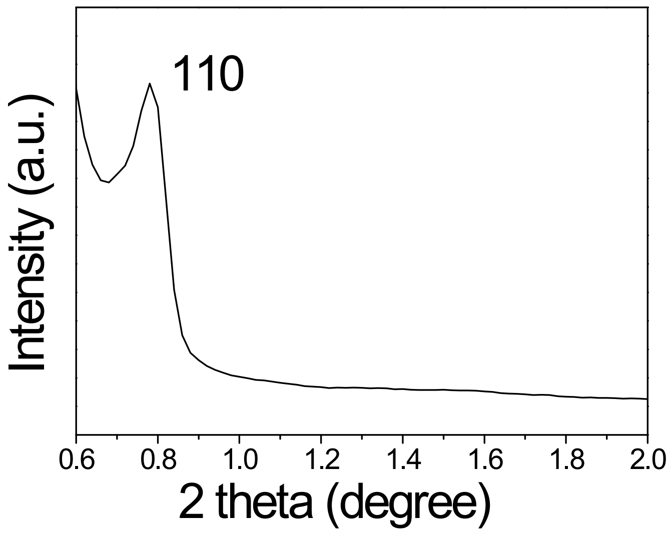

Fig. S1. Small-angle XRD pattern of the ordered mesoporous carbon FDU-16.

4 TGA of Ni/OMC

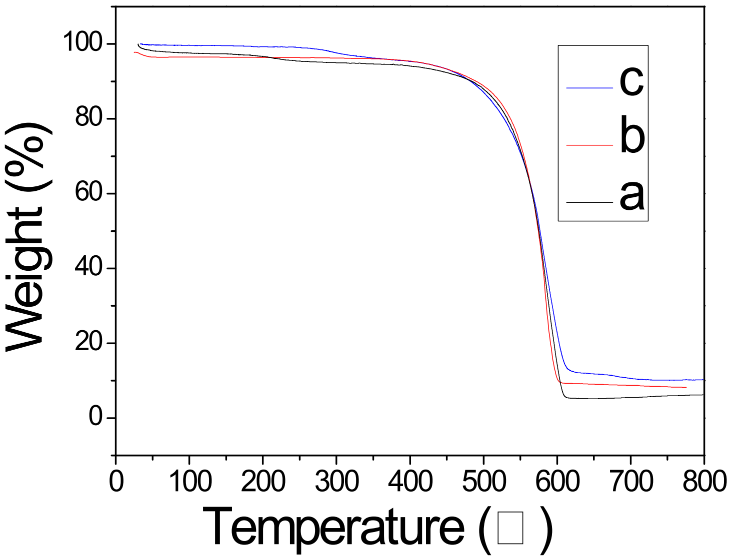

Fig. S2. TGA curves of the Ni nanoparticles/OMC composites with different Ni contents: (a) Ni/OMC-0.05, (b) Ni/OMC-0.075, (c) Ni/OMC-0.1.

5 BET of FDU-16 and Ni/OMC.

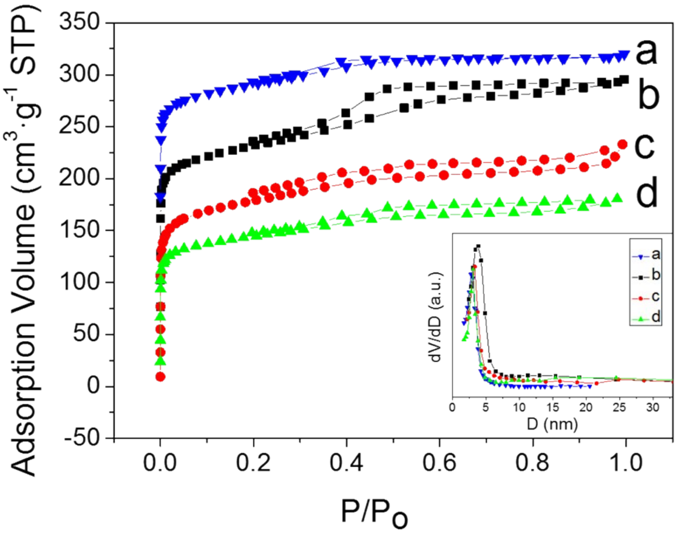

Fig. S3. N_2 sorption/desorption isotherms and the corresponding pore size distribution curve (inset) of the Ni nanoparticles/OMC composites with different Ni contents: (a) FDU-16, (b) Ni/OMC-0.05, (c) Ni/OMC-0.075, (d) Ni/OMC-0.1.

6 Magnified TEM of Ni/OMC

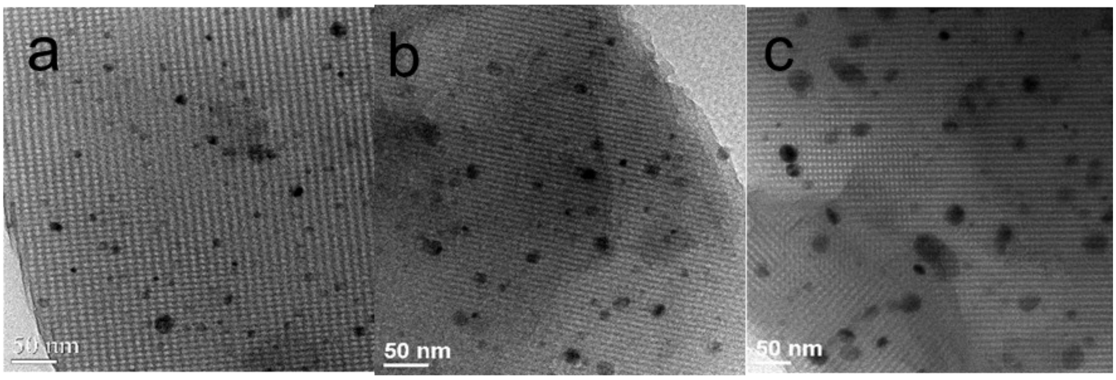

Fig. S4. Magnified TEM images of the Ni nanoparticle/OMC composites: (a) Ni/OMC-0.05, (b) Ni/OMC-0.075 and (c) Ni/OMC-0.1.

7 EDX-Mapping of Ni/OMC

Ni/OMC-0.05

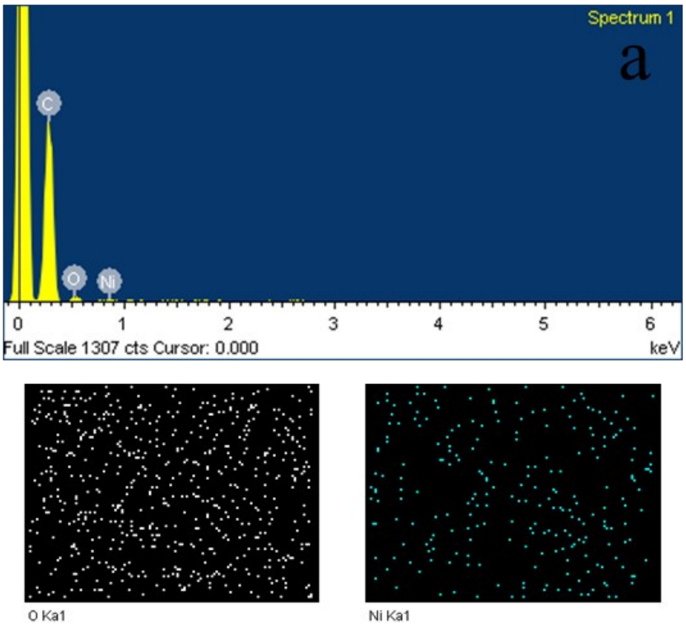

Ni/OMC-0.075

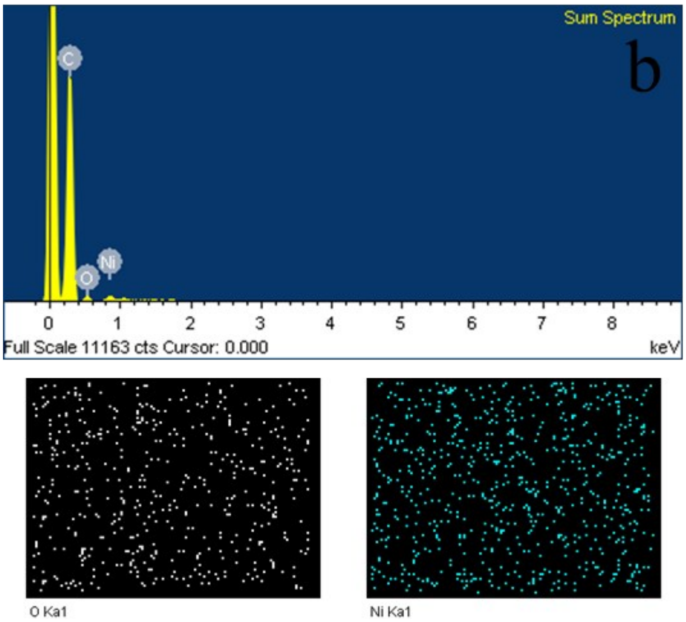

Ni/OMC-0.1

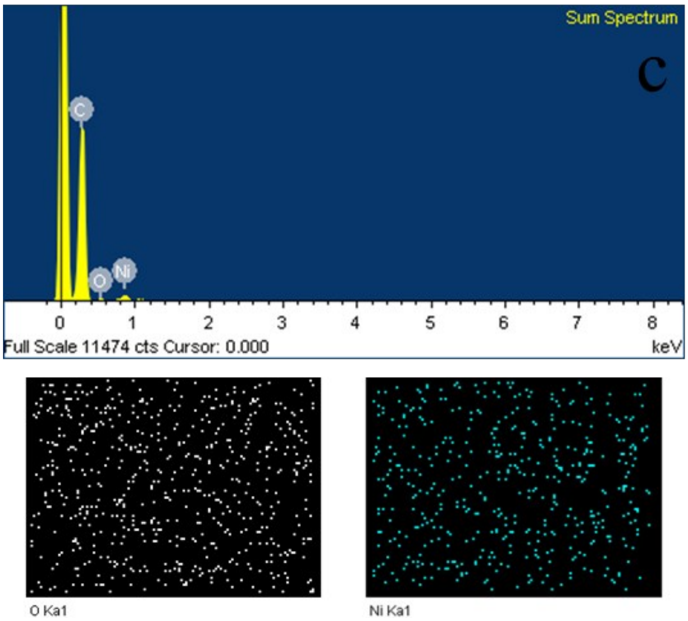

Fig. S5. EDX-Mapping images of the Ni nanoparticle/OMC composites: (a) Ni/OMC-0.05, (b) Ni/OMC-0.075 and (c) Ni/OMC-0.1.

8 Characterization of Ni/OMC-0.1 after using 7 times

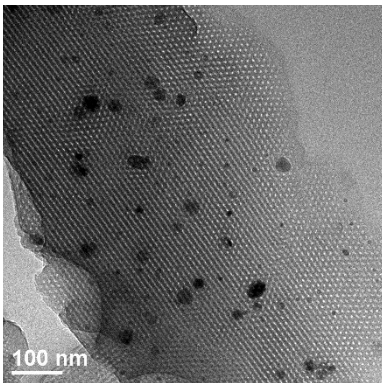

Fig. S6. TEM images of Ni/OMC-0.1 after using 7 times.

9 Characterization of Ni/OMC-0.1 with different carbonization temperature

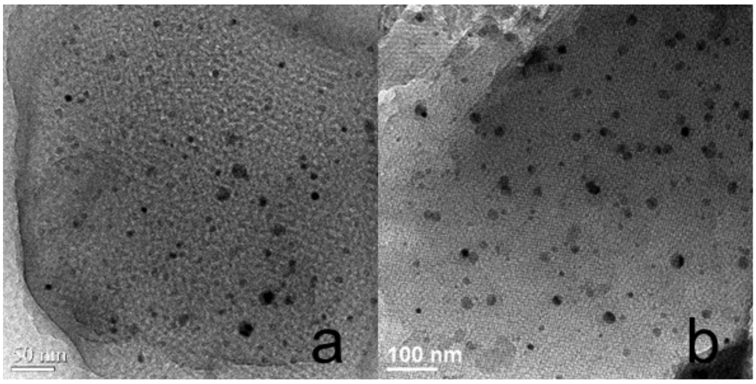

Fig. S7. TEM images of Ni/OMC-0.1 with different carbonization temperature: (a) Ni/OMC-0.1 carbonized at 600°C and (b) Ni/OMC-0.1 carbonized at 750°C.

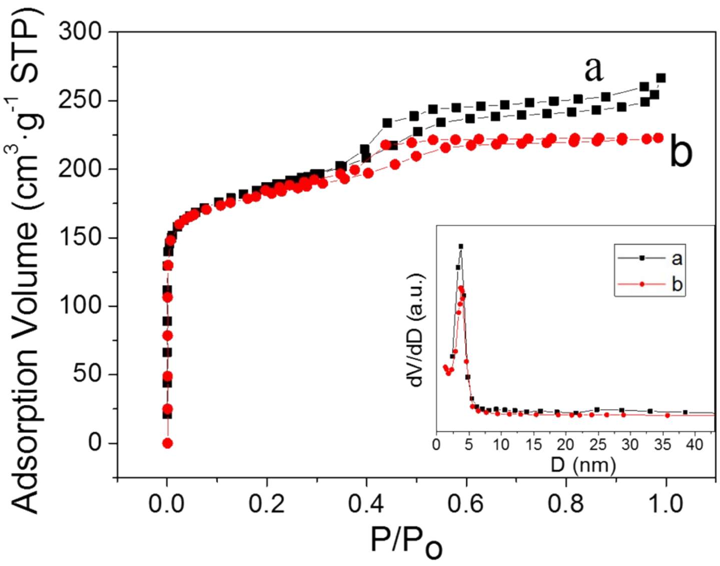

Fig. S8. N_2 sorption/desorption isotherms and the corresponding pore size distribution curve (inset) of OMC/Ni-0.1 with different carbonization temperature: (a) Ni/OMC-0.1 carbonized at 600°C, (b) Ni/OMC-0.1 carbonized at 750°C.

Table S1. Textural properties of Ni/OMC-0.1 with different carbonization temperature

Carbonization temperature	**S_{BET} ^{a} ($m^2 \cdot g^{-1}$)**	**Vp^a ($cm^3 \cdot g^{-1}$)**	**Dp^b (nm)**
600°C	654	0.41	3.7
750°C	625	0.34	3.7

a Calculated by the BJH model from sorption data in a relative pressure range from 0.04 to 0.2.

b Calculated by the BJH model from the adsorption branches of the isotherms.

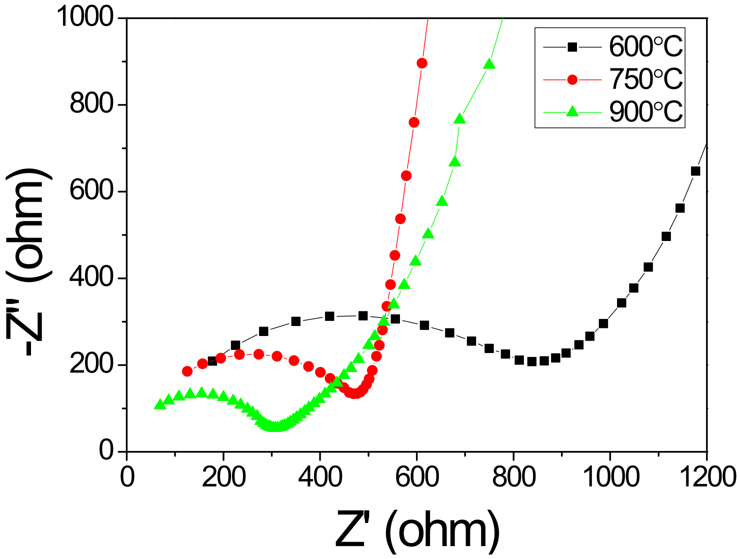

Fig. S9. Nyquist plots of electrochemical impedance spectroscopy (EIS) for Ni/OMC-0.1 with different carbonization temperature.

Electrochemical impedance measurements were performed in a mixture of substrate aromatic ketone 1 (0.005 M) and supporting electrolyte TEABr (0.1 M) in 10 ml of DMF in an undivided glass cell with a perturbation amplitude 0.3 mV over a frequency range of 0.01 Hz to 100 kHz. The cell was equipped with a monolithic Ni/OMC as cathode and platinum filament as anode.

10 Characterization of Ni/OMC-0.1 (3h)

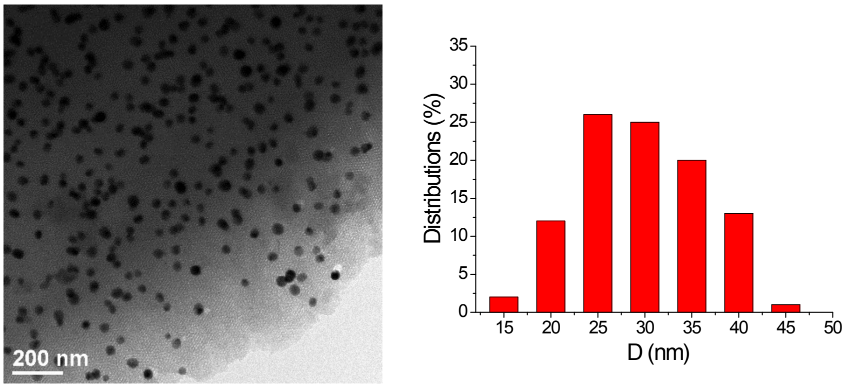

Fig. S10. TEM images and the corresponding particle size distributions of the nickle nanoparticles of Ni/OMC-0.1 with stirring time (3h).

Table S2. Textural properties of Ni/OMC-0.1 with stirring time (3h)

stirring time (h)	**S_{BET} ^{a} ($m^2 \cdot g^{-1}$)**	**Vp^{a} ($cm^3 \cdot g^{-1}$)**	**Dp^{b} (nm)**
3	392	0.23	2.7

a Calculated by the BJH model from sorption data in a relative pressure range from 0.04 to 0.2.

b Calculated by the BJH model from the adsorption branches of the isotherms.